

# Insights into voltage-gated calcium channel regulation from the structure of the $\text{Ca}_V1.2$ IQ domain– $\text{Ca}^{2+}$ /calmodulin complex

Filip Van Petegem, Franck C Chatelain & Daniel L Minor, Jr

Changes in activity-dependent calcium flux through voltage-gated calcium channels ( $\text{Ca}_V$ s) drive two self-regulatory calcium-dependent feedback processes that require interaction between  $\text{Ca}^{2+}$ /calmodulin ( $\text{Ca}^{2+}/\text{CaM}$ ) and a  $\text{Ca}_V$  channel consensus isoleucine-glutamine (IQ) motif: calcium-dependent inactivation (CDI) and calcium-dependent facilitation (CDF). Here, we report the high-resolution structure of the  $\text{Ca}^{2+}/\text{CaM}$ – $\text{Ca}_V1.2$  IQ domain complex. The IQ domain engages hydrophobic pockets in the N-terminal and C-terminal  $\text{Ca}^{2+}/\text{CaM}$  lobes through sets of conserved ‘aromatic anchors.’  $\text{Ca}^{2+}/\text{N}$  lobe adopts two conformations that suggest inherent conformational plasticity at the  $\text{Ca}^{2+}/\text{N}$  lobe–IQ domain interface. Titration calorimetry experiments reveal competition between the lobes for IQ domain sites. Electrophysiological examination of  $\text{Ca}^{2+}/\text{N}$  lobe aromatic anchors uncovers their role in  $\text{Ca}_V1.2$  CDF. Together, our data suggest that  $\text{Ca}_V$  subtype differences in CDI and CDF are tuned by changes in IQ domain anchoring positions and establish a framework for understanding CaM lobe-specific regulation of  $\text{Ca}_V$ s.

Voltage-gated calcium channels are the ion channels that define excitable cells<sup>1</sup>. These channels control cellular calcium entry in response to changes in membrane potential and are pivotal in the generation of cardiac action potentials, excitation-contraction coupling, hormone and neurotransmitter release and activity-dependent transcription initiation<sup>1,2</sup>.  $\text{Ca}_V$ s are multisubunit complexes composed of three essential channel subunits<sup>2</sup>,  $\text{Ca}_V\alpha_1$ ,  $\text{Ca}_V\beta$  and  $\text{Ca}_V\alpha_2\delta$ , plus the ubiquitous intracellular calcium sensor calmodulin (CaM)<sup>3</sup>. An additional subunit,  $\text{Ca}_V\gamma$ , is associated with skeletal muscle channels, but its general importance in other tissues is unsettled<sup>4</sup>.

The  $\text{Ca}_V\alpha_1$  subunits are single polypeptide chains of ~1,800–2,200 residues in which the ion-conducting pore is formed from four homologous repeats that each bear six transmembrane segments<sup>2</sup>. There are three  $\text{Ca}_V$  subfamilies, which have diverse physiological and pharmacological properties that depend largely on the  $\text{Ca}_V\alpha_1$ -subunit:  $\text{Ca}_V1.x$  (L-type),  $\text{Ca}_V2.x$  (2.1, P/Q-type; 2.2, N-type; 2.3, R-type) and  $\text{Ca}_V3.x$  (T-type)<sup>1</sup>. Large interdomain intracellular loops bridge the four transmembrane repeats of the  $\text{Ca}_V\alpha_1$  subunit and serve as docking sites for auxiliary subunits and regulatory molecules that control channel activity and connect  $\text{Ca}_V$  channels to larger macromolecular complexes and cellular signaling pathways<sup>5,6</sup>.

Calcium influx is a potent activator of intracellular signaling pathways but is toxic in excess<sup>1,7</sup>. Because  $\text{Ca}_V$ s are major sources of calcium influx,  $\text{Ca}_V$  activity is strongly controlled by both self-regulatory and extrinsic mechanisms that tune channel action in response to electrical excitation, neurotransmitter stimulation and

hormonal cues<sup>1,2,8</sup>. This intense regulation uses multiple mechanisms and classes of intracellular signaling molecules. The bi-lobed calcium sensor CaM has a preeminent role in the intrinsic mechanisms of  $\text{Ca}_V$  calcium-dependent regulation<sup>9–15</sup>. Activity-dependent changes in intracellular calcium levels from flux through  $\text{Ca}_V$  channel pores drive two self-regulatory calcium-dependent feedback mechanisms that limit or enhance calcium entry through the channel: CDI and CDF<sup>8</sup>. Both require the interaction of  $\text{Ca}^{2+}/\text{CaM}$  with a consensus IQ motif in the  $\text{Ca}_V\alpha_1$  C-terminal cytoplasmic tail<sup>9,11–16</sup>.

Multiple lines of evidence suggest that CaM is constitutively tethered to the channel to detect calcium in the vicinity of the channel pore<sup>12,17,18</sup> and to permit calcium ions to exert control over their own entry through  $\text{Ca}_V$ s. The nature of the tethering site remains unclear. It may comprise a region immediately adjacent to the IQ domain on the N-terminal side, termed the Pre-IQ region<sup>17,19,20</sup>, or a composite of the Pre-IQ and IQ domain<sup>18,20</sup>.

The IQ domain is believed to be the site of action of  $\text{Ca}^{2+}/\text{CaM}$ . Numerous studies show that  $\text{Ca}^{2+}/\text{CaM}$  binds IQ peptides from different  $\text{Ca}_V$  channels *in vitro*<sup>9,11–14,17,20–22</sup> and that IQ domain mutations in full-length channels can eliminate CDI<sup>9,13–15,23</sup> and CDF<sup>9,14</sup>.

Although CDI and CDF are well documented, the details are complex, differ among channel subtypes and have not been readily predictable given the primary-sequence similarities among the  $\text{Ca}_V$  CaM-binding domains. Elegant experiments have demonstrated that CDI and CDF are controlled independently by the abilities of the

Cardiovascular Research Institute, Department of Biochemistry and Biophysics and Department of Cellular and Molecular Pharmacology, California Institute for Quantitative Biomedical Research, University of California, San Francisco, 1700 4th St., Box 2532, San Francisco, California 94143-2532, USA. Correspondence should be addressed to D.L.M. (daniel.minor@ucsf.edu).

Received 4 October; accepted 26 October; published online 20 November 2005; doi:10.1038/nsmb1027

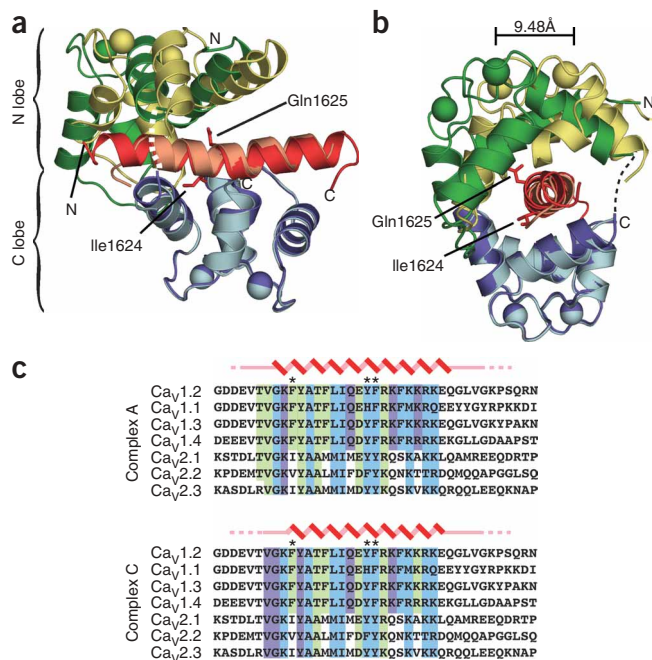


**Figure 1** Structure of the  $\text{Ca}^{2+}/\text{CaM}$ - $\text{Ca}_V1.2$  IQ domain complex. **(a)** Ribbon diagram of the complex. Green, CaM  $\text{Ca}^{2+}/\text{N}$  lobe; blue,  $\text{Ca}^{2+}/\text{C}$  lobe; red, IQ domain, with residues Ile1624 and Q1625 from complex A in stick representation; darker shades, complex A; lighter shades, complex C. The complexes were superposed using the  $\text{Ca}^{2+}/\text{C}$  lobes and IQ domains. Labels indicate termini of components in complex A. Dashed lines indicate regions absent from the structures. **(b)**  $90^\circ$  rotation of **a**. The shift in  $\text{Ca}^{2+}/\text{N}$  lobe  $\text{Ca}^{2+}$  position in EF-hand 2 is indicated. **(c)** Sequence alignment of IQ regions from each  $\text{Ca}_V1$  and  $\text{Ca}_V2$  isoform. Zigzag,  $\alpha$ -helical regions; straight line, nonhelical residues; dashed lines, residues present in the crystallized construct but absent from the electron density. Residues contacting CaM ( $\leq 4 \text{ \AA}$ ) for conformation A and conformation C are highlighted as follows: green, contacts to  $\text{Ca}^{2+}/\text{N}$  lobe; cyan,  $\text{Ca}^{2+}/\text{C}$  lobe; purple,  $\text{Ca}^{2+}/\text{N}$  lobe and  $\text{Ca}^{2+}/\text{C}$  lobe. Asterisks indicate principal aromatic anchor positions. Sequences are human  $\text{Ca}_V1.2$  1609–1647, human  $\text{Ca}_V1.1$  1514–1552, rat  $\text{Ca}_V1.3$  1641–1679, human  $\text{Ca}_V1.4$  1563–1602, human  $\text{Ca}_V2.1$  1947–1985, human  $\text{Ca}_V2.2$  1845–1883 and rat  $\text{Ca}_V2.3$  1811–1850.

N-terminal and C-terminal CaM lobes (the N lobe and C lobe) to bind calcium<sup>9,10,12,16,23</sup>. CDI is present in both L-type ( $\text{Ca}_V1.2$ ) and non-L-type ( $\text{Ca}_V2.1$ ,  $\text{Ca}_V2.2$  and  $\text{Ca}_V2.3$ ) channels but arises from the action of opposite CaM lobes in these two cases<sup>9,23</sup>. In the L-type channel  $\text{Ca}_V1.2$ , CDI is governed by the binding of calcium ions to the C lobe<sup>12</sup>, whereas in non-L-type channels ( $\text{Ca}_V2$ s), CDI is triggered by the binding of calcium ions to the N lobe<sup>9,11,23</sup>. In the non-L-type channel  $\text{Ca}_V2.1$ , CDF arises from interactions between calcium ions and the C lobe. Despite the fact that the C lobe-mediated processes elicit different channel behaviors in different channel subtypes, CDI in L-type and CDF in non-L-type channels, both C lobe processes share insensitivity to the fast calcium chelator BAPTA<sup>23</sup>. This shared resistance suggests that in both cases the C lobe captures calcium that is local to the channel pore<sup>23</sup>. In contrast,  $\text{Ca}_V2$  N lobe-mediated CDF is sensitive to the slow calcium chelator EGTA, suggesting that it detects global changes in calcium concentration<sup>9,23</sup>. These lobe-specific

calcium sensitivities have been suggested to provide mechanisms for  $\text{Ca}_V$ s to sense, decode and distinguish local calcium changes due to calcium permeation through the channel from global calcium changes due to aggregate cellular signals<sup>9,23</sup>.

To delineate the ways in which CDI and CDF arise, we set out to determine the molecular basis for  $\text{Ca}^{2+}/\text{CaM}$  interactions. Here, we report the high-resolution crystal structure of the human  $\text{Ca}^{2+}/\text{CaM}$ - $\text{Ca}_V1.2$  IQ domain complex. By using the structural data to inform functional experiments, we uncover an unexpected competition between the  $\text{Ca}^{2+}/\text{CaM}$  lobes for a common site on the IQ domain and demonstrate a previously unknown role for the  $\text{Ca}^{2+}/\text{N}$  lobe anchors in  $\text{Ca}_V1.2$  CDF. This structure provides the first insight into the molecular machinery that underlies  $\text{Ca}^{2+}/\text{CaM}$  regulation of  $\text{Ca}_V$ s.

## RESULTS

### Structure of the $\text{Ca}^{2+}/\text{CaM}$ - $\text{Ca}_V1.2$ IQ domain complex

We solved the crystal structure of the  $\text{Ca}^{2+}/\text{CaM}$ - $\text{Ca}_V1.2$  IQ domain complex at 2.00- $\text{\AA}$  resolution using a three-wavelength MAD experiment on a selenomethionine (SeMet)-substituted protein crystal. The asymmetric unit contains three independent 1:1  $\text{Ca}^{2+}/\text{CaM}$ -IQ domain complexes (complexes A, B and C) that have two principal conformations, represented by complexes A and C (Fig. 1a,b). Complex B is similar to complex A but has poorly defined density for the C-terminal half of the IQ domain (Supplementary Fig. 1 online).

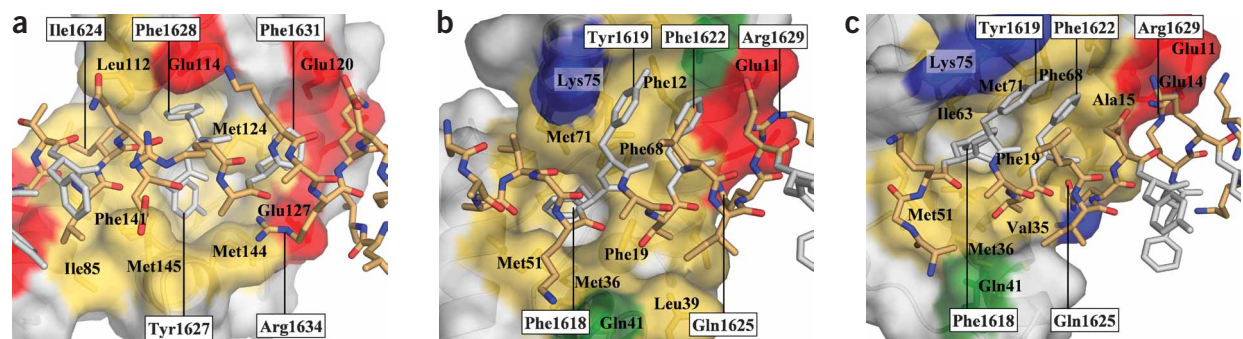


**Figure 2** Lobe-specific  $\text{Ca}^{2+}/\text{CaM}$ - $\text{Ca}_V1.2$  IQ domain interactions. **(a)**  $\text{Ca}^{2+}/\text{CaM}$  C lobe from complex A bound to the IQ domain. Buried surface area = 1,819  $\text{\AA}^2$  (965  $\text{\AA}^2$  hydrophobic). **(b)**  $\text{Ca}^{2+}/\text{CaM}$  N lobe from complex A bound to the IQ domain. Buried surface area = 1,450  $\text{\AA}^2$  (743  $\text{\AA}^2$  hydrophobic). **(c)**  $\text{Ca}^{2+}/\text{CaM}$  N lobe from complex C bound to the IQ domain. Buried surface area = 1,491  $\text{\AA}^2$  (500  $\text{\AA}^2$  hydrophobic). IQ domain is shown in stick representation with aromatic anchor residues in white. CaM lobes are shown in surface representation with residues that contribute hydrophobic (yellow), negatively charged (red), positively charged (blue) and polar (green) side chain contacts ( $\leq 4 \text{ \AA}$ ) to the IQ domain indicated. Select residues are labeled to orient the reader. IQ domain residue labels are boxed.

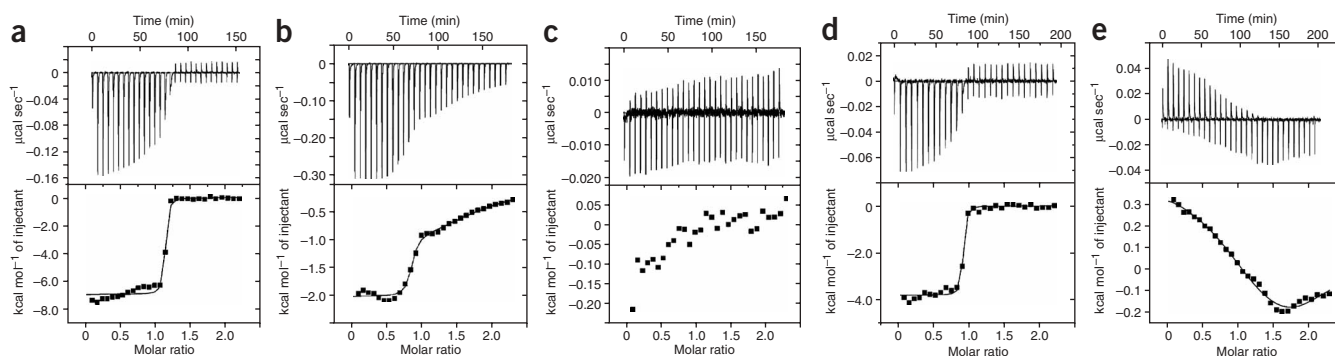


**Figure 3** ITC characterization of  $\text{Ca}^{2+}/\text{CaM}$ - $\text{CaV}1.2$  IQ domain interactions. (a)  $70 \mu\text{M}$  IQ domain into  $7 \mu\text{M}$   $\text{Ca}^{2+}/\text{C}$  lobe. (b)  $500 \mu\text{M}$   $\text{Ca}^{2+}/\text{N}$  lobe into  $50 \mu\text{M}$  IQ domain. (c)  $200 \mu\text{M}$   $\text{Ca}^{2+}/\text{N}$  lobe into a solution of  $20 \mu\text{M}$  IQ domain and  $37 \mu\text{M}$  C lobe. (d)  $60 \mu\text{M}$  IQ domain F1628A mutant into  $6 \mu\text{M}$   $\text{Ca}^{2+}/\text{C}$  lobe. (e)  $500 \mu\text{M}$   $\text{Ca}^{2+}/\text{N}$  lobe into a solution of  $5 \mu\text{M}$  IQ domain F1628A mutant. Isotherms are fit to a single binding site model for **a** and **d** and a double binding site model for **b** and **e**. Panels show addition of  $10 \mu\text{l}$  aliquots of titrant into the target solution (top) and binding isotherms (bottom).

Thus, our analysis focuses on the well-defined structures of complexes A and C. Both are compact structures in which  $\text{Ca}^{2+}/\text{CaM}$  embraces the largely  $\alpha$ -helical IQ domain in a parallel orientation (Fig. 1a,b) through extensive interactions that involve twenty-two (complex A) or twenty-one (complex C) contiguous residues in the IQ domain, and both bury  $\sim 3,100 \text{ \AA}^2$  total surface area of which roughly  $1,650 \text{ \AA}^2$  is hydrophobic (Fig. 1c). The observed parallel orientation in which  $\text{Ca}^{2+}/\text{N}$  lobe binds the N-terminal portion of the target helix and  $\text{Ca}^{2+}/\text{C}$  lobe binds the C-terminal portion is unusual and known in only one other  $\text{Ca}^{2+}/\text{CaM}$  peptide structure, the  $\text{Ca}^{2+}/\text{CaM}$ -dependent kinase peptide complex<sup>24,25</sup>. A high density of positively charged side chains project from the  $\text{CaV}1.2$  IQ helix near the C terminus and make electrostatic interactions with negatively charged residues that ring the  $\text{Ca}^{2+}/\text{CaM}$  exit tunnel (Fig. 2). These interactions are consistent with the proposal that the distribution of positive charges on  $\text{Ca}^{2+}/\text{CaM}$ -binding peptides is an important determinant of binding orientation<sup>24</sup>.

The  $\text{Ca}^{2+}/\text{C}$  lobes of complexes A and C are nearly identical (r.m.s. deviation for  $C\alpha$  atoms is 0.475) and are anchored similarly to the IQ domain helix (Figs. 1 and 2). The  $\text{Ca}^{2+}/\text{N}$  lobes are also similar (r.m.s. deviation for  $C\alpha$  atoms is 0.97) and have only small changes in the positions of side chains involved in direct contacts with the IQ peptide (Supplementary Fig. 2 online). Superposition of  $\text{Ca}^{2+}/\text{C}$  lobes and IQ helices shows that the  $\text{Ca}^{2+}/\text{N}$  lobe adopts two distinct binding modes (Fig. 1a,b). In complex A, the  $\text{Ca}^{2+}/\text{N}$  lobe is positioned further along the N-terminal end of the IQ domain, whereas in complex C, the  $\text{Ca}^{2+}/\text{N}$  lobe is tilted and shifted toward the C-terminal end of

the IQ domain, leading to a more compact conformation. The conformational differences cause relative displacements in the positions of the two  $\text{Ca}^{2+}$  ions in the  $\text{Ca}^{2+}/\text{N}$  lobe EF-hands of  $\sim 8.6 \text{ \AA}$  and  $\sim 9.5 \text{ \AA}$  and increase the bend present in both IQ domain helices at Ile1624 by  $\sim 10^\circ$  in complex C.

#### Aromatic anchors mediate IQ domain- $\text{Ca}^{2+}/\text{CaM}$ contacts

The  $\text{CaV}1.2$  IQ helix engages  $\text{Ca}^{2+}/\text{CaM}$  through a set of ‘aromatic anchor’ residues. The C-terminal portion of the IQ helix displays three aromatic anchors (Tyr1627, Phe1628 and Phe1631) that bind hydrophobic  $\text{Ca}^{2+}/\text{C}$  lobe pockets. Two anchors (Tyr1627 and Phe1628) are deeply buried (Fig. 2a). The N-terminal part of the IQ helix presents three aromatic residues (Phe1618, Tyr1619 and Phe1622) that make hydrophobic interactions with the  $\text{Ca}^{2+}/\text{N}$  lobe; these residues reside on the opposite helical face from the C-terminal anchors. Phe1618 makes the most extensive contacts and binds a deep hydrophobic pocket (Fig. 2b,c). Despite the alternative positions of the  $\text{Ca}^{2+}/\text{N}$  lobe, Phe1618 remains buried in the same  $\text{Ca}^{2+}/\text{N}$  lobe hydrophobic pocket in both complexes by adopting different side chain rotamers (Fig. 2b,c and Supplementary Fig. 2).

#### $\text{Ca}^{2+}/\text{CaM}$ interactions with IQ domain consensus residues

IQ domains are defined by the consensus sequence (I/L/V) QXXXRXXX(R/K) (where X is any residue)<sup>26,27</sup>. The  $\text{Ca}^{2+}/\text{CaM}$ - $\text{CaV}1.2$  structure reveals the ways in which the hallmark residues of the IQ domain interact with the  $\text{Ca}^{2+}/\text{CaM}$  lobes. The Ile1624 side chain

**Table 1** Thermodynamic parameters for  $\text{CaV}1.2$  IQ domain- $\text{Ca}^{2+}/\text{CaM}$  lobe interactions

	WT- $\text{Ca}^{2+}/\text{C}$ lobe	WT- $\text{Ca}^{2+}/\text{N}$ lobe	F1628A- $\text{Ca}^{2+}/\text{C}$ lobe	F1628A- $\text{Ca}^{2+}/\text{N}$ lobe
$N_1$	$0.98 \pm 0.18$	$0.85 \pm 0.05$	$0.92 \pm 0.04$	$0.96 \pm 0.13$
$K_{d1}$ (nM)	$2.63 \pm 0.07$	$57.6 \pm 35.5$	$2.59 \pm 0.24$	$1,003 \pm 567$
$\Delta H_1$ (kcal mol <sup>-1</sup> )	$-6.77 \pm 0.21$	$-1.91 \pm 0.14$	$-3.69 \pm 0.17$	$0.45 \pm 0.02$
$\Delta S_1$ (cal mol <sup>-1</sup> K <sup>-1</sup> )	$15.75 \pm 0.78$	$26.70 \pm 0.85$	$26.45 \pm 0.78$	$29.20 \pm 1.13$
$\Delta G_1$ (kcal mol <sup>-1</sup> )	$-11.31 \pm 0.01$	$-9.60 \pm 0.38$	$-11.31 \pm 0.06$	$-7.96 \pm 0.35$
$N_2$		$1.04 \pm 0.0$		$1.0 \pm 0.0$
$K_{d2}$ (nM)		$19,190 \pm 3,600$		$9,812 \pm 8,220$
$\Delta H_2$ (kcal mol <sup>-1</sup> )		$-1.42 \pm 0.13$		$-0.67 \pm 0.22$
$\Delta S_2$ (cal mol <sup>-1</sup> K <sup>-1</sup> )		$16.60 \pm 0.84$		$21.00 \pm 2.69$
$\Delta G_2$ (kcal mol <sup>-1</sup> )		$-6.20 \pm 0.11$		$-6.71 \pm 0.55$

Thermodynamic parameters of  $\text{Ca}^{2+}/\text{C}$  lobe and  $\text{Ca}^{2+}/\text{N}$  lobe binding to wild-type (WT) and F1628A  $\text{CaV}1.2$  IQ domain at pH 7.4 in the presence of  $1 \text{ mM}$   $\text{CaCl}_2$ . Each value corresponds to the mean of two separate experiments with different batches of both components ( $\pm$  s.d.).

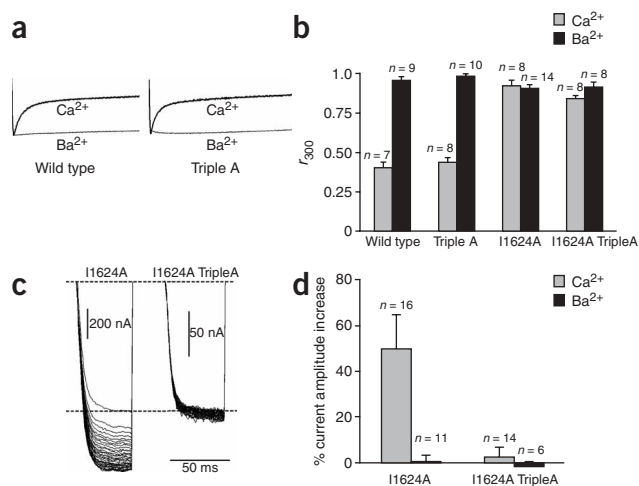


**Figure 4** Lobe-specific interactions affect CDI and CDF. **(a)** Voltage-activated  $\text{Ba}^{2+}$  and  $\text{Ca}^{2+}$  currents from wild-type (WT) and TripleA channels during a 600-ms depolarizing step from  $-90$  mV to  $+20$  mV. Traces are normalized to the peak current to facilitate comparison. Tail currents are not shown. **(b)**  $r_{300}$  values (current fraction 300 ms after depolarization) in  $\text{Ba}^{2+}$  (black) and  $\text{Ca}^{2+}$  (grey). Error bars show s.d. **(c)** I1624A and I1624A TripleA  $\text{Ca}^{2+}$  currents in a 3-Hz 40-pulse train (50-ms steps to  $+20$ -mV from  $-90$ -mV holding potential). The first pulse currents are scaled to the same level for comparison. **(d)** Relative current increase between last and first pulses for I1624A and I1624A TripleA. Error bars show s.d.

is completely buried (solvent-exposed area =  $0.7 \text{ \AA}^2$ ) and contacts the hydrophobic surface of the C lobe (Fig. 2a and Supplementary Figs. 2 and 3 online). The Gln1625 side chain has many contacts to the  $\text{Ca}^{2+}$ /N lobe. This residue also makes side chain and main chain water-mediated hydrogen bonds to the  $\text{Ca}^{2+}$ /C lobe (Supplementary Figs. 2 and 3). The central arginine, Arg1629, and terminal basic residue, Arg1634, form salt bridges with Glu11 and Glu14 of the  $\text{Ca}^{2+}$ /N lobe (Supplementary Figs. 2 and 3) and Glu127 of the  $\text{Ca}^{2+}$ /C lobe (Supplementary Fig. 3), respectively. Thus, all IQ hallmark residues seem important for IQ domain– $\text{Ca}^{2+}$ /CaM interactions. These residues, together with the aromatic anchors and other positions throughout the IQ domain, establish the extensive network of contacts in the complex (Supplementary Fig. 3).

### Isothermal titration calorimetry

We used isothermal titration calorimetry (ITC) to gain insight into the thermodynamics of lobe-specific  $\text{Ca}^{2+}$ /CaM–IQ domain interactions (Fig. 3).  $\text{Ca}^{2+}$ /C lobe binds the IQ domain with 1:1 stoichiometry and a high affinity ( $K_d = 2.63 \times 10^{-9}$  M) that is driven by favorable enthalpic and entropic contributions (Fig. 3a and Table 1). Similar favorable components drive  $\text{Ca}^{2+}$ /N lobe binding; however, the isotherms revealed that there are two different binding sites, a medium-affinity ( $K_d = 5.76 \times 10^{-8}$  M) and low-affinity ( $K_d = 1.92 \times 10^{-5}$  M) site (Fig. 3b and Table 1). Both  $\text{Ca}^{2+}$ /N lobe–IQ domain interactions are substantially weaker than the  $\text{Ca}^{2+}$ /C lobe–IQ domain interaction. Titration of  $\text{Ca}^{2+}$ /N lobe into a solution containing  $\text{Ca}^{2+}$ /C lobe–IQ domain complexes yielded no further binding energy (Fig. 3c). These data directly demonstrate that the high-affinity  $\text{Ca}^{2+}$ /C lobe–IQ domain interaction occludes both measurable  $\text{Ca}^{2+}$ /N lobe-binding sites.

To investigate further whether the  $\text{Ca}^{2+}$ /N lobe- and  $\text{Ca}^{2+}$ /C lobe-binding sites depend on interactions observed in the crystal structure, we examined the consequence of a mutation in the IQ domain's

aromatic anchor for  $\text{Ca}^{2+}$ /C lobe, F1628A. The F1628A mutant binds  $\text{Ca}^{2+}$ /C lobe with an affinity that is identical to the wild-type domain ( $K_d = 2.59 \times 10^{-9}$  M), but with a reduced enthalpy (Fig. 3d and Table 1). This type of enthalpy-entropy compensation is a common feature in protein-protein interactions<sup>28</sup> and reflects a loss of key interactions in the bound state that is compensated by increased disorder. In contrast, the F1628A mutation causes a substantial perturbation of  $\text{Ca}^{2+}$ /N lobe medium-affinity binding ( $K_d = 1.003 \times 10^{-6}$  M for F1628A compared to  $K_d = 5.76 \times 10^{-8}$  M for the wild-type domain) and causes an unfavorable binding enthalpy. These data directly demonstrate that the medium-affinity  $\text{Ca}^{2+}$ /N lobe-binding site requires interactions with residues that comprise the crystallographically observed  $\text{Ca}^{2+}$ /C lobe site.

### N lobe anchors have a role in CDF

Although  $\text{Ca}^{2+}$ /C lobe has an established role in  $\text{Ca}_v1.2$  CDI<sup>12,16,17</sup>, no role has yet been defined for  $\text{Ca}^{2+}$ /N lobe. Therefore, we tested whether the crystallographically observed  $\text{Ca}^{2+}$ /N lobe interface has a role in channel function by using two-electrode voltage clamp to interrogate mutant channels that were heterologously expressed in *Xenopus laevis* oocytes. A triple mutant lacking the three aromatic anchors for  $\text{Ca}^{2+}$ /N lobe (F1618A Y1619A F1622A), 'TripleA,' showed no appreciable difference in  $\text{Ca}_v1.2$  inactivation when either  $\text{Ca}^{2+}$  or  $\text{Ba}^{2+}$  was the charge carrier (Fig. 4a,b). Thus,  $\text{Ca}^{2+}$ /N lobe–aromatic anchor interactions do not seem important for  $\text{Ca}_v1.2$  CDI. This result agrees with the observation that overexpression of the CaM mutant CaM<sub>12</sub>, in which the N lobe EF-hands have diminished calcium binding, has little effect on CDI<sup>12,16</sup>. TripleA channels consistently gave lower current amplitudes compared to wild-type channels. Previous reports have suggested a role for the IQ domain in  $\text{Ca}_v$  trafficking<sup>29</sup>; our observation raises the possibility that aromatic anchors for  $\text{Ca}^{2+}$ /N lobe may be important in this process.

Because the aromatic anchors for  $\text{Ca}^{2+}$ /N lobe are not crucial for  $\text{Ca}_v1.2$  CDI, we asked whether they might have a role in CDF. CDF is a prominent property of  $\text{Ca}_v2.1$  channels<sup>9,10,30</sup>. Although CDF is not readily detectable in wild-type  $\text{Ca}_v1.2$  channels, robust CDF is unmasked by the I1624A mutation<sup>14,15</sup>. The I1624A mutation in the TripleA background (I1624A TripleA) results in channels lacking both CDI (Fig. 4b) and CDF (Fig. 4c,d). Lowering expression of a I1624A-only mutant such that current magnitudes were equivalent to those of the I1624A TripleA mutant still produced clear CDF (data not shown). This result excludes the possibility that CDF loss in I1624A TripleA is a consequence of the lower current magnitudes. Together, these experiments suggest that the aromatic anchors for the  $\text{Ca}^{2+}$ /N lobe have a previously unappreciated role in  $\text{Ca}_v1.2$  CDF.

### DISCUSSION

Calcium ions are potent chemical effectors of many cellular processes<sup>1,7</sup>. The opening of  $\text{Ca}_v$ s in response to changes in membrane potential is a major source of calcium influx<sup>1</sup> and thus couples two forms of biological signals, electrical and chemical. The  $\text{Ca}_v$  activity that drives this powerful signaling combination is subject to a variety of control mechanisms. A diverse set of proteins that includes auxiliary channel subunits, G-proteins, synaptic vesicle components, kinases, phosphatases and calcium sensors interact with and modify the behavior of the pore-forming subunit to limit or enhance calcium influx<sup>1,2</sup>.

Two types of feedback regulation in which calcium ions affect their own entry through  $\text{Ca}_v$ s and control local calcium levels have been intensively studied for more than two decades<sup>8</sup>. CDI, which limits

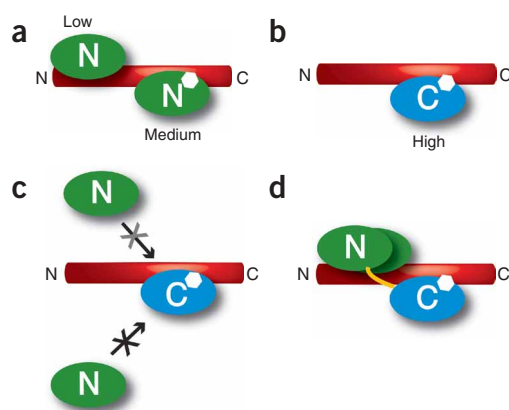


**Figure 5** Schematic of  $\text{Ca}^{2+}/\text{CaM}$  lobe multiple binding modes on the  $\text{Ca}_v1.2$  IQ domain. (a)  $\text{Ca}^{2+}/\text{N}$  lobe (green) has medium-affinity and low-affinity binding sites on the IQ domain. (b)  $\text{Ca}^{2+}/\text{C}$  lobe (blue) has a high-affinity binding site on the IQ domain. (c) Binding of  $\text{Ca}^{2+}/\text{C}$  lobe to the IQ domain blocks  $\text{Ca}^{2+}/\text{N}$  lobe access to the  $\text{Ca}^{2+}/\text{N}$  lobe medium-affinity site (black X) and reduces  $\text{Ca}^{2+}/\text{N}$  lobe binding to the  $\text{Ca}^{2+}/\text{N}$  lobe low-affinity site (grey X). (d) Representation of how  $\text{Ca}^{2+}/\text{C}$  lobe binding to the IQ domain tethers  $\text{Ca}^{2+}/\text{N}$  lobe near the  $\text{Ca}^{2+}/\text{N}$  lobe low-affinity site. Yellow line indicates the CaM interlobe linker. In all panels, the approximate position of aromatic anchor Phe1628, which is shared by the  $\text{Ca}^{2+}/\text{N}$  lobe medium-affinity site and the  $\text{Ca}^{2+}/\text{C}$  lobe high-affinity site, is indicated by the white hexagon.

calcium flux through  $\text{Ca}_v\text{s}$ , and CDF, which enhances calcium flux through  $\text{Ca}_v\text{s}$ , both result from interactions between calcium ions, a channel-resident CaM and the  $\text{Ca}_v\alpha_1$  subunit's C-terminal cytoplasmic IQ domain<sup>9,11–16,31</sup>. Further dissection of the molecular origins of CDI and CDF has shown that each process arises from the binding of specific calcium-bound CaM lobes to the IQ domain<sup>10,12–14</sup>; however, the precise details have remained unknown.

IQ domains are protein segments that contain the 11-residue consensus sequence (I/L/V)QXXXRXXX(R/K) and comprise a family of  $\text{Ca}^{2+}/\text{CaM}$ - and apo CaM-binding motifs found in diverse proteins including molecular motors, voltage-gated calcium channels, voltage-gated sodium channels and phosphatases<sup>26,27</sup>. The  $\text{Ca}^{2+}/\text{CaM}$ -IQ domain structure presented here offers the first high-resolution picture of the molecular details of a  $\text{Ca}^{2+}/\text{CaM}$ -IQ domain interaction. A previous work has proposed that Ile1624 is exposed in the  $\text{Ca}^{2+}/\text{CaM}$ - $\text{Ca}_v1.2$  complex to provide hydrophobic contacts to other parts of the channel-gating machinery<sup>32</sup>. Contrary to this prediction, the structure shows that Ile1624 is completely buried (solvent-exposed area =  $0.7 \text{ \AA}^2$ ) and contacts the hydrophobic surface of the C lobe (Fig. 2a and Supplementary Figs. 2 and 3). Other hallmark residues of the IQ domain engage in extensive hydrophobic and polar interactions with the CaM lobes that establish the importance of these residues for the  $\text{Ca}^{2+}/\text{CaM}$ -IQ domain interaction (Fig. 1 and Supplementary Figs. 2 and 3).

The aromatic anchors that form the IQ domain's principal contacts to the  $\text{Ca}^{2+}/\text{CaM}$  lobes were not anticipated from prior studies. Comparison of the  $\text{Ca}_v$  IQ domain defined by the crystal structure with other IQ motifs reveals that many anchor positions are unique to  $\text{Ca}_v\text{s}$ . Such an array of aromatic anchors, particularly the N-terminal anchors, is lacking in the C-terminal cytoplasmic IQ domains of the closely related family of voltage-gated sodium channels ( $\text{Na}_v\text{s}$ )<sup>33–35</sup> (Supplementary Fig. 4 online). This observation suggests that CaM binding to  $\text{Ca}_v$  and  $\text{Na}_v$  IQ domains and subsequent modulatory

effects may be fundamentally different despite overall similarities in  $\text{Na}_v$  and  $\text{Ca}_v$  architecture<sup>1</sup>.

Examination of the  $\text{Ca}^{2+}/\text{CaM}$ - $\text{Ca}_v1.2$  IQ domain complexes shows interesting differences in the ways  $\text{Ca}^{2+}/\text{N}$  lobe and  $\text{Ca}^{2+}/\text{C}$  lobe interact with the IQ domain: the number of binding conformations differs, with two for  $\text{Ca}^{2+}/\text{N}$  lobe versus one for  $\text{Ca}^{2+}/\text{C}$  lobe; the number of deep anchor positions differs, with one for  $\text{Ca}^{2+}/\text{N}$  lobe (Phe1618) versus two for  $\text{Ca}^{2+}/\text{C}$  lobe (Tyr1627 and Phe1628); and the buried surface areas are not equivalent, as  $\text{Ca}^{2+}/\text{C}$  lobe buries more total and more hydrophobic surface than  $\text{Ca}^{2+}/\text{N}$  lobe (Fig. 2). These differences suggest that the  $\text{Ca}^{2+}/\text{C}$  lobe binds more tightly to the IQ domain. As it is not simple to infer directly the energetic importance of molecular interactions from structural data alone<sup>36</sup>, we pursued experiments to determine whether these observed differences in modes of interaction have functional consequences.

We used ITC to probe the binding between the individual CaM lobes and the IQ domain. ITC experiments directly determine the thermodynamic parameters that underlie binding reactions and provide a degree of resolution for studying macromolecular interactions that is unmatched by other methods<sup>37</sup>. The experiments showed that the  $\text{Ca}^{2+}/\text{C}$  lobe binds the IQ domain with high affinity ( $K_d = 2.6 \text{ nM}$ ). To our surprise, we found multiple binding sites for the  $\text{Ca}^{2+}/\text{N}$  lobe on the IQ domain (Fig. 5a). The lack of appreciable  $\text{Ca}^{2+}/\text{N}$  lobe binding to the  $\text{Ca}^{2+}/\text{C}$  lobe-IQ domain complex (Fig. 3c), together with the large reduction in  $\text{Ca}^{2+}/\text{N}$  lobe binding affinity by the aromatic-anchor mutation F1628A (Fig. 3e), indicates that the medium-affinity  $\text{Ca}^{2+}/\text{N}$  lobe-binding site overlaps directly with the  $\text{Ca}^{2+}/\text{C}$  lobe-binding site (Fig. 5). The competition experiment (Fig. 3c) also showed that the binding of  $\text{Ca}^{2+}/\text{C}$  lobe to the IQ domain lowers the affinity of the second  $\text{Ca}^{2+}/\text{N}$  lobe-binding site to an undetectable level ( $K_d > 200 \text{ }\mu\text{M}$ , given the concentrations used in the experiment<sup>37</sup>). The dominance of  $\text{Ca}^{2+}/\text{C}$  lobe in IQ domain binding energetics agrees with the eminent role of the  $\text{Ca}^{2+}/\text{C}$  lobe in CDI of L-type channels<sup>12,16,17</sup>. Given that the medium-affinity  $\text{Ca}^{2+}/\text{N}$  lobe site overlaps with the high-affinity  $\text{Ca}^{2+}/\text{C}$  lobe site and that  $\text{Ca}^{2+}/\text{C}$  lobe binding to its high-affinity site weakens the avidity of  $\text{Ca}^{2+}/\text{N}$  lobe for its low-affinity site, the thermodynamic data suggest that the crystallographically observed  $\text{Ca}^{2+}/\text{N}$  lobe interactions correspond to the  $\text{Ca}^{2+}/\text{N}$  lobe low-affinity site. These interactions arise from the high effective concentration<sup>38</sup> of the  $\text{Ca}^{2+}/\text{N}$  lobe relative to the peptide caused by  $\text{Ca}^{2+}/\text{C}$  lobe binding and the CaM interlobe linker (Fig. 5d).

As  $\text{Ca}^{2+}/\text{C}$  lobe binds tighter than  $\text{Ca}^{2+}/\text{N}$  lobe to the site that includes Phe1628,  $\text{Ca}^{2+}/\text{N}$  lobe is not expected to occupy this part of the IQ domain when both CaM lobes are loaded with calcium. However,  $\text{Ca}^{2+}/\text{N}$  lobe may occupy this position in channel functional states in which the N lobe is loaded with calcium but the C lobe is in the apo state. This property may be particularly relevant for  $\text{Ca}_v2\text{s}$ , where functional experiments have demonstrated that CaM mutants that have diminished C lobe calcium binding but preserve N lobe calcium binding maintain CDI<sup>9,11,23</sup>.

Functional studies indicate lobe-specific tasks for CaM in  $\text{Ca}_v$  regulation<sup>9,12,16,17,23</sup>. The interactions that bring about lobe-specific regulation by CaM have remained obscure despite the investigation of an abundance of mutations to the IQ domain<sup>13–15,17,18,32</sup>. In the context of the structure, it is clear that most of the reported  $\text{Ca}_v1.2$  mutants, many of which involve multiple residue changes, alter contacts to both lobes simultaneously and therefore cannot be used to decipher the roles of binding to each lobe individually. The exceptions are mutants having changes at two single positions that contact the  $\text{Ca}^{2+}/\text{C}$  lobe, Ile1624 and Phe1628 (refs. 14,15). Ile1624

mutations that perturb the residue's hydrophobicity and size disrupt CDI<sup>15</sup>. F1628A changes channel inactivation properties<sup>15</sup>. Together, these results indicate that the crystallographically defined IQ domain interface that contacts the Ca<sup>2+</sup>/C lobe is important for channel inactivation.

Both CaM lobes have specific functional roles in modulation of Ca<sub>v</sub>2 channels<sup>9,11,23</sup>. There is a clear role for the Ca<sup>2+</sup>/C lobe in Ca<sub>v</sub>1 CDI. Ca<sub>v</sub>1s and Ca<sub>v</sub>2s are highly homologous in the region that interacts with CaM to mediate CDF and CDI. Despite the similarity, no role has yet been reported for the N lobe in Ca<sub>v</sub>1 modulation. We tested whether the Ca<sup>2+</sup>/N lobe-anchoring residues observed in the Ca<sup>2+</sup>/CaM-IQ domain structure had a functional role. Simultaneous mutation of all three aromatic anchors for the N lobe to alanine did not affect Ca<sub>v</sub>1.2 CDI (Fig. 4a,b). In contrast, these same mutations in the background of the I1624A mutation, which un.masks Ca<sub>v</sub>1.2 CDF, completely disrupted Ca<sub>v</sub>1.2 CDF, demonstrating a clear role for this Ca<sup>2+</sup>/N lobe interface in CDF (Fig. 4c,d). These experiments define a previously unknown role for the N lobe interface and suggest that the Ca<sup>2+</sup>/N lobe conformations seen in the structure are important for CDF. Apo CaM can also bind the IQ domain<sup>18,20</sup>. It remains possible that the functional effects we observed have more complex origins that arise from interplay between Ca<sup>2+</sup>/CaM- and apo CaM-IQ domain binding.

The dual binding mode of Ca<sup>2+</sup>/N lobe observed in the structure suggests a level of conformational plasticity in Ca<sup>2+</sup>/N lobe-channel interactions. Regions on the N-terminal side of the IQ domain bind Ca<sup>2+</sup>/CaM *in vitro*<sup>17,19–21,39</sup>, but with lower affinity than the IQ domain does<sup>17,20</sup>. Anchoring of the Ca<sup>2+</sup>/C lobe to the IQ domain may permit Ca<sup>2+</sup>/CaM to remain bound while other regions of the channel compete for Ca<sup>2+</sup>/N lobe or the Ca<sup>2+</sup>/N lobe aromatic anchors during various states of channel operation<sup>17,39,40</sup>. Alternatively, the observed conformational plasticity may provide a means for the complex to accommodate conformational changes that facilitate interactions with other channel domains while maintaining the Ca<sup>2+</sup>/N lobe-IQ interaction.

Ca<sub>v</sub>2s show lobe-specific Ca<sup>2+</sup>/CaM modulation that seems inverted relative to Ca<sub>v</sub>1.2 (refs. 9,11,23). Ca<sub>v</sub>2 CDI relies on the Ca<sup>2+</sup>/N lobe<sup>9,11,23</sup>, whereas the prominent CDF of Ca<sub>v</sub>2.1 originates with the Ca<sup>2+</sup>/C lobe<sup>9,11</sup>. The ITC data show that the Ca<sup>2+</sup>/N lobe-binding sites in the Ca<sub>v</sub>1.2 IQ domain overlap with the Ca<sup>2+</sup>/C lobe-binding site. It is notable that three aromatic anchors identified here, Phe1618, Phe1622 and Phe1631, including Ca<sup>2+</sup>/N lobe aromatic anchor Phe1618, are conserved among Ca<sub>v</sub>1s but not between Ca<sub>v</sub>1s and Ca<sub>v</sub>2s (Fig. 1c). Amino acid substitutions at these positions, together with changes at Gln1625 and Lys1633 (Fig. 1c), may tilt the Ca<sup>2+</sup>/N lobe- and Ca<sup>2+</sup>/C lobe-IQ domain affinity differences in favor of the Ca<sup>2+</sup>/N lobe. Such changes, in concert with interactions to other parts of the channel, may underlie the fundamental differences in lobe-specific modulation between Ca<sub>v</sub>1.2 and Ca<sub>v</sub>2s in a

way that exploits the prodigious adaptability of CaM to recognize varied targets<sup>41</sup>.

The Ca<sup>2+</sup>/CaM-Ca<sub>v</sub>1.2 IQ domain structure presented here is the first high-resolution view of the components that transduce Ca<sup>2+</sup>-dependent Ca<sub>v</sub> regulation, and it provides a necessary molecular framework for detailed dissection of the transitions that drive the rich regulation of Ca<sub>v</sub>s by CaM.

## METHODS

**Purification.** The IQ domain of human Ca<sub>v</sub>1.2 (Ca<sub>v</sub>α<sub>1c</sub>77) (residues 1611–1644), human CaM N lobe (residues 1–78) and human CaM C lobe (residues 79–148) were cloned into a modified pET28 vector (Novagen) denoted HMT<sup>42</sup> that contains, in sequence, a His<sub>6</sub>-tag, maltose-binding protein and a cleavage site for the tobacco etch virus (TEV) protease. Full-length CaM was cloned into pEGST<sup>43</sup> without using any affinity tag. The F1628A mutation in the IQ domain was obtained using the QuikChange protocol (Stratagene).

All proteins were expressed in *Escherichia coli* BL21(DE3)pLysS grown in 2× YT media at 37 °C. Cells were lysed in 250 mM KCl, 10 mM K-HEPES (pH 7.4) and 1 mM CaCl<sub>2</sub> (buffer A) supplemented with 1 mM PMSF. The complex of CaM and IQ domain was obtained by coexpression and was purified on a Poros20MC column (PerSeptive Biosystems), washed with buffer A and eluted with buffer A plus 500 mM imidazole (buffer B). After cleavage with His-tagged TEV protease<sup>44</sup> at room temperature for ~12 h and dialysis against 100 mM KCl, 10 mM Tris-HCl (pH 8.8) and 1 mM CaCl<sub>2</sub> (buffer C), the complex was purified on a Hiload HQ column (Amersham) in buffer C with a linear gradient to 30% buffer D (1 M KCl, 10 mM Tris-HCl (pH 8.8), 1 mM CaCl<sub>2</sub>). Trace amounts of residual maltose-binding protein were removed by collecting the flow-through from an additional passage of the purified material over a

**Table 2** Data collection, phasing and refinement statistics

	Native		SeMet	
<b>Data collection</b>				
Space group	<i>P</i> 2 <sub>1</sub>		<i>P</i> 2 <sub>1</sub>	
Cell dimensions				
<i>a</i> , <i>b</i> , <i>c</i> (Å)	84.73, 37.24, 86.86		82.55, 37.01, 87.55	
$\alpha$ , $\beta$ , $\gamma$ (°)	90, 97.77, 90		90, 98.10, 90	
		<i>Peak</i>	<i>Inflection</i>	<i>Remote</i>
Wavelength	1.116	0.97957	0.97972	1.01986
Resolution (Å)	30.0–2.0 (2.07–2.0)	30–2.5 (2.59–2.50)	30–2.8 (2.90–2.80)	30–2.4 (2.49–2.40)
<i>R</i> <sub>sym</sub>	6.6 (33.1)	9.5 (42.8)	7.4 (40.1)	6.6 (34.3)
<i>I</i> / $\sigma$ <i>I</i>	19.8 (2.2)	19.0 (2.5)	14.2 (2.1)	15.0 (1.7)
Completeness (%)	99.2 (98.3)	97.1 (99.4)	99.9 (100)	87.1 (89.6)
Redundancy	3.5	7.8	3.8	2.6
<b>Refinement</b>				
Resolution (Å)	30.0–2.0			
No. reflections	36,436			
<i>R</i> <sub>work</sub> / <i>R</i> <sub>free</sub>	20.23 / 25.47			
No. atoms				
Protein	3,845			
Ligand/ion	15			
Water	260			
<i>B</i> -factors				
Protein	31.50			
Ligand/ion	38.16			
Water	47.05			
R.m.s. deviations				
Bond lengths (Å)	0.016			
Bond angles (°)	1.363			

One native and one SeMet crystal were used for structure solution. Highest-resolution shell is shown in parentheses.

Poros20MC column in buffer A. Finally, the sample was dialyzed against 20 mM KCl, 10 mM K-HEPES (pH 7.4) and 1 mM CaCl<sub>2</sub>.

SeMet-substituted complex was expressed in BL21(DE3)pLysS cells in M9 minimal medium containing 20% (w/v) glucose, with the methionine biosynthesis pathway inhibited<sup>45</sup>. Purification was as described above with all buffers supplemented with 5 mM methionine and 10 mM β-mercaptoethanol.

The first steps of purifying HMT-CaM N lobe and HMT-CaM C lobe fusions were similar to the CaM-IQ domain purification. After TEV cleavage, the material was dialyzed against buffer E (10 mM Tris-HCl (pH 8.8), 10 mM KCl, 1 mM CaCl<sub>2</sub>) and purified on a HiLoad HQ column with a gradient from 0 to 50% buffer F (1 M KCl, 10 mM Tris-HCl (pH 8.8), 1 mM CaCl<sub>2</sub>). The proteins were purified further on a Poros20MC column in buffer A, and the concentrated flow-through was applied to a TSK2000 column (Tosoh Biosep) run in buffer A.

To obtain free IQ domain we purified the complex with CaM as described above and separated the two components on a preparative C18 HPLC column (Vydac) with a linear gradient from 35 to 50% acetonitrile in 0.1% (v/v) trifluoroacetic acid over 15 column volumes. The purity was verified by MALDI-TOF mass spectrometry.

**Crystallization and structure determination.** Complexes of native and SeMet-substituted CaM-IQ domain were crystallized by sitting or hanging drop vapor diffusion<sup>46</sup> at 20 °C by mixing equal volumes of protein (~10 mg ml<sup>-1</sup>) and well solution containing 0.1 M Bis-Tris (pH 6.5) and 20–30% (w/v) PEG 3350. After transfer to Paratone oil (Hampton Research) and flash-freezing, diffraction data were collected at Beamline 8.3.1 (Advanced Light Source, Lawrence Berkeley National Laboratories) and processed using HKL2000 (ref. 47). A three-wavelength MAD experiment was performed on crystals of SeMet-substituted protein (Table 2). Twenty-five initial selenium positions were located using ShelxD<sup>48</sup>. Subsequent refinement, substructure completion and phasing were performed using SHARP<sup>49</sup> (Supplementary Fig. 1). After density modification the figure of merit was 0.852. An initial model was built using RESOLVE<sup>50</sup> and ARP/wARP<sup>51</sup>, manually extended with XtalView<sup>52</sup> and refined against 2.00-Å native data using REFMAC5 (ref. 53). TLS parameters were used throughout the refinement. Side chains and full residues with missing electron densities were not modeled. The final model consists of three Ca<sup>2+</sup>/CaM-IQ domain complexes in the asymmetric unit with 95.2% of the residues in the core region of the Ramachandran plot and none in disallowed regions. A Ni<sup>2+</sup> ion is observed in all three complexes and most likely was introduced into the sample from the Ni<sup>2+</sup> affinity column (Poros20MC). Its presence in the crystal was confirmed by a fluorescence wavelength scan. The Ni<sup>2+</sup> binds at the C lobe outer surface distal from the IQ domain and is not expected to interfere with Ca<sup>2+</sup>/CaM-IQ domain binding. Refinement data and statistics are shown in Table 2.

**Isothermal titration calorimetry.** Samples were concentrated and dialyzed twice against 5 mM KCl, 10 mM HEPES (pH 7.4) and 1 mM CaCl<sub>2</sub>. Higher salt concentrations reduced the solubility of the IQ domain. Samples were degassed for 5 min and titrations were performed on a VP-ITC calorimeter (MicroCal) at 15 °C. Data were processed with MicroCal Origin 7.0. For fitting of the F1628A N lobe data, the stoichiometry for the second binding site was set equal to 1. Because of the high titrant concentration required to measure weak interactions, and owing to limited solubility of the IQ domain, N lobe was titrated into peptide and not vice versa.

Protein concentrations were determined by absorbance<sup>54</sup>, except for N lobe CaM (which has no aromatic residues), where the BCA method was used, using known concentrations of full-length CaM and CaM C lobe as references. Each ITC experiment was repeated with different batches of purified protein, yielding similar thermodynamic parameters and stoichiometry values. Control injections, consisting of titrating one component into buffer, were used to adjust the baseline of each experiment.

**Electrophysiology.** Constructs for electrophysiology consisted of human Cav1.2 (splice variant α<sub>1c77</sub>) in pcDNA3.1(+)/hygro (Invitrogen), Cavβ<sub>2a</sub> in pGEM (Promega) and rabbit Cavα<sub>2δ</sub> in pcDNA3 (Invitrogen). Mutants of the α<sub>1c77</sub> subunit were made using the QuikChange protocol (Stratagene). RNA transcripts were prepared using a T7 mMessage mMachine kit (Ambion). 50 nl of a complementary RNA mixture containing 30–100 nM Cav1.2 α<sub>1c77</sub>, 33 nM

Cavβ<sub>2a</sub> and 33 nM Cavα<sub>2δ</sub> was microinjected into *Xenopus* oocytes, which were then kept at 18 °C in ND96 medium supplemented with penicillin and streptomycin. Recordings were performed 3–7 d after injection. Before recording, oocytes were injected with 25–50 nl 100 mM BAPTA to minimize contaminating Ca<sup>2+</sup>-activated Cl<sup>-</sup> current. During recordings, the oocytes were superfused using a Valvelink 16 (Automate Scientific) controller with either a Ba<sup>2+</sup>-containing solution (40 mM Ba(OH)<sub>2</sub>, 50 mM NaOH, 1 mM KOH, 0.4% (w/v) niflumic acid, 10 mM HEPES) or a Ca<sup>2+</sup>-containing solution (Ba(OH)<sub>2</sub> replaced with Ca(NO<sub>3</sub>)<sub>2</sub>). Both solutions were adjusted to pH 7.4 using HNO<sub>3</sub>. Two-electrode voltage-clamp experiments were performed using a GeneClamp 500B amplifier (Axon Instruments) controlled by a computer with a 1,200 MHz processor (Celeron, Gateway) using CLAMPEX 8.2.0.224 (Axon Instruments) and digitized at 1 kHz with a Digidata1332A (Axon Instruments). Electrodes were filled with 3 M KCl and had resistances of 0.1–1.5 MΩ. Leak currents were subtracted using a P/4 protocol. Ionic currents were analyzed with Clampfit 8.2 (Axon Instruments).

**Accession codes.** Protein Data Bank: Coordinates have been deposited with accession code 2BE6.

*Note: Supplementary information is available on the Nature Structural & Molecular Biology website.*

#### ACKNOWLEDGMENTS

We thank K. Brejc and D. Fass for comments on the manuscript; J. Holton at Beamline 8.3.1 at the Advanced Light Source for help with data collection; C.B. Klee (US National Institutes of Health, Bethesda, Maryland, USA) for the calmodulin clone; R.W. Tsien (Stanford University School of Medicine, Stanford, California, USA) and D.T. Yue (Johns Hopkins University School of Medicine, Baltimore, USA) for calcium channel clones; and members of the Minor laboratory for support at all stages of this work. This work was supported by awards to D.L.M. from the McKnight Foundation for Neuroscience, the Rita Allen Foundation, the Alfred P. Sloan Foundation and the US National Institutes of Health and to F.V.P. from the American Heart Association Western States Affiliate. D.L.M. is a McKnight Scholar in Neurosciences, an Alfred P. Sloan Research Fellow and a Rita Allen Foundation Scholar.

#### COMPETING INTERESTS STATEMENT

The authors declare that they have no competing financial interests.

Published online at <http://www.nature.com/nsmb/>

Reprints and permissions information is available online at <http://npg.nature.com/reprintsandpermissions/>

- Hille, B. *Ion Channels of Excitable Membranes* (Sinauer Associates, Inc., Sunderland, Massachusetts, USA, 2001).
- Catterall, W.A. Structure and regulation of voltage-gated Ca<sup>2+</sup> channels. *Annu. Rev. Cell Dev. Biol.* **16**, 521–555 (2000).
- Saimi, Y. & Kung, C. Calmodulin as an ion channel subunit. *Annu. Rev. Physiol.* **64**, 289–311 (2002).
- Kang, M.G. & Campbell, K.P. Gamma subunit of voltage-activated calcium channels. *J. Biol. Chem.* **278**, 21315–21318 (2003).
- Sheng, Z.H., Westenbroek, R.E. & Catterall, W.A. Physical link and functional coupling of presynaptic calcium channels and the synaptic vesicle docking/fusion machinery. *J. Bioenerg. Biomembr.* **30**, 335–345 (1998).
- Walker, D. & De Waard, M. Subunit interaction sites in voltage-dependent Ca<sup>2+</sup> channels: role in channel function. *Trends Neurosci.* **21**, 148–154 (1998).
- Kandel, E.R., Schwartz, J.H. & Jessell, T.M. *Principles of Neural Science* (McGraw-Hill, New York, USA, 2000).
- Budde, T., Meuth, S. & Pape, H.C. Calcium-dependent inactivation of neuronal calcium channels. *Nat. Rev. Neurosci.* **3**, 873–883 (2002).
- DeMaria, C.D., Soong, T.W., Alseikhan, B.A., Alvania, R.S. & Yue, D.T. Calmodulin bifurcates the local Ca<sup>2+</sup> signal that modulates P/Q-type Ca<sup>2+</sup> channels. *Nature* **411**, 484–489 (2001).
- Lee, A. *et al.* Ca<sup>2+</sup>/calmodulin binds to and modulates P/Q-type calcium channels. *Nature* **399**, 155–159 (1999).
- Lee, A., Zhou, H., Scheuer, T. & Catterall, W.A. Molecular determinants of Ca<sup>2+</sup>/calmodulin-dependent regulation of Cav2.1 channels. *Proc. Natl. Acad. Sci. USA* **100**, 16059–16064 (2003).
- Peterson, B.Z., DeMaria, C.D., Adelman, J.P. & Yue, D.T. Calmodulin is the Ca<sup>2+</sup> sensor for Ca<sup>2+</sup>-dependent inactivation of L-type calcium channels. *Neuron* **22**, 549–558 (1999).
- Qin, N., Olcese, R., Bransby, M., Lin, T. & Birnbaumer, L. Ca<sup>2+</sup>-induced inhibition of the cardiac Ca<sup>2+</sup> channel depends on calmodulin. *Proc. Natl. Acad. Sci. USA* **96**, 2435–2438 (1999).

14. Zühlke, R.D., Pitt, G.S., Deisseroth, K., Tsien, R.W. & Reuter, H. Calmodulin supports both inactivation and facilitation of L-type calcium channels. *Nature* **399**, 159–162 (1999).
15. Zühlke, R.D., Pitt, G.S., Tsien, R.W. & Reuter, H. Ca<sup>2+</sup>-sensitive inactivation and facilitation of L-type Ca<sup>2+</sup> channels both depend on specific amino acid residues in a consensus calmodulin-binding motif in the (alpha)1C subunit. *J. Biol. Chem.* **275**, 21121–21129 (2000).
16. Alseikhan, B.A., DeMaria, C.D., Colecraft, H.M. & Yue, D.T. Engineered calmodulins reveal the unexpected eminence of Ca<sup>2+</sup> channel inactivation in controlling heart excitation. *Proc. Natl. Acad. Sci. USA* **99**, 17185–17190 (2002).
17. Pitt, G.S. *et al.* Molecular basis of calmodulin tethering and Ca<sup>2+</sup>-dependent inactivation of L-type Ca<sup>2+</sup> channels. *J. Biol. Chem.* **276**, 30794–30802 (2001).
18. Erickson, M.G., Liang, H., Mori, M.X. & Yue, D.T. FRET two-hybrid mapping reveals function and location of L-type Ca<sup>2+</sup> channel CaM preassociation. *Neuron* **39**, 97–107 (2003).
19. Romanin, C. *et al.* Ca(2+) sensors of L-type Ca(2+) channel. *FEBS Lett.* **487**, 301–306 (2000).
20. Tang, W. *et al.* Apocalmodulin and Ca<sup>2+</sup> calmodulin-binding sites on the Cav1.2 channel. *Biophys. J.* **85**, 1538–1547 (2003).
21. Pate, P. *et al.* Determinants for calmodulin binding on voltage-dependent Ca<sup>2+</sup> channels. *J. Biol. Chem.* **275**, 39786–39792 (2000).
22. Black, D.J. *et al.* Calmodulin interactions with IQ peptides from voltage-dependent calcium channels. *Am. J. Physiol. Cell Physiol.* **288**, C669–C676 (2005).
23. Liang, H. *et al.* Unified mechanisms of Ca(2+) regulation across the Ca(2+) channel family. *Neuron* **39**, 951–960 (2003).
24. Osawa, M. *et al.* A novel target recognition revealed by calmodulin in complex with Ca<sup>2+</sup>-calmodulin-dependent kinase. *Nat. Struct. Biol.* **6**, 819–824 (1999).
25. Kurokawa, H. *et al.* Target-induced conformational adaptation of calmodulin revealed by the crystal structure of a complex with nematode Ca(2+)/calmodulin-dependent kinase kinase peptide. *J. Mol. Biol.* **312**, 59–68 (2001).
26. Bahler, M. & Rhoads, A. Calmodulin signaling via the IQ motif. *FEBS Lett.* **513**, 107–113 (2002).
27. Jurado, L.A., Chockalingam, P.S. & Jarrett, H.W. Apocalmodulin. *Physiol. Rev.* **79**, 661–682 (1999).
28. Dunitz, J.D. Win some, lose some: enthalpy-entropy compensation in weak intermolecular interactions. *Chem. Biol.* **2**, 709–712 (1995).
29. Gao, T., Bunemann, M., Gerhardstein, B.L., Ma, H. & Hosey, M.M. Role of the C terminus of the alpha 1C (Cav1.2) subunit in membrane targeting of cardiac L-type calcium channels. *J. Biol. Chem.* **275**, 25436–25444 (2000).
30. Lee, A., Scheuer, T. & Catterall, W.A. Ca<sup>2+</sup>/calmodulin-dependent facilitation and inactivation of P/Q-type Ca<sup>2+</sup> channels. *J. Neurosci.* **20**, 6830–6838 (2000).
31. Zühlke, R.D. & Reuter, H. Ca<sup>2+</sup>-sensitive inactivation of L-type Ca<sup>2+</sup> channels depends on multiple cytoplasmic amino acid sequences of the alpha1C subunit. *Proc. Natl. Acad. Sci. USA* **95**, 3287–3294 (1998).
32. Kim, J., Ghosh, S., Nunziato, D.A. & Pitt, G.S. Identification of the components controlling inactivation of voltage-gated Ca<sup>2+</sup> channels. *Neuron* **41**, 745–754 (2004).
33. Deschenes, I. *et al.* Isoform-specific modulation of voltage-gated Na(+) channels by calmodulin. *Circ. Res.* **90**, E49–E57 (2002).
34. Kim, J. *et al.* Calmodulin mediates Ca<sup>2+</sup> sensitivity of sodium channels. *J. Biol. Chem.* **279**, 45004–45012 (2004).
35. Mori, M. *et al.* Novel interaction of the voltage-dependent sodium channel (VDSC) with calmodulin: does VDSC acquire calmodulin-mediated Ca<sup>2+</sup>-sensitivity? *Biochemistry* **39**, 1316–1323 (2000).
36. Clackson, T. & Wells, J.A. A hot spot of binding energy in a hormone-receptor interface. *Science* **267**, 383–386 (1995).
37. Leavitt, S. & Freire, E. Direct measurement of protein binding energetics by isothermal titration calorimetry. *Curr. Opin. Struct. Biol.* **11**, 560–566 (2001).
38. Jencks, W.P. On the attribution of additivity of binding energies. *Proc. Natl. Acad. Sci. USA* **78**, 4046–4050 (1981).
39. Mouton, J., Feltz, A. & Maulet, Y. Interactions of calmodulin with two peptides derived from the c-terminal cytoplasmic domain of the Ca(v)1.2 Ca<sup>2+</sup> channel provide evidence for a molecular switch involved in Ca<sup>2+</sup>-induced inactivation. *J. Biol. Chem.* **276**, 22359–22367 (2001).
40. Xiong, L., Kleerekoper, Q.K., He, R., Putkey, J.A. & Hamilton, S.L. Sites on calmodulin that interact with the C-terminal tail of Cav1.2 channel. *J. Biol. Chem.* **280**, 7070–7079 (2005).
41. Hoeflich, K.P. & Ikura, M. Calmodulin in action: diversity in target recognition and activation mechanisms. *Cell* **108**, 739–742 (2002).
42. Van Petegem, F., Clark, K.A., Chatelain, F.C. & Minor, D.L., Jr. Structure of a complex between a voltage-gated calcium channel beta-subunit and an alpha-subunit domain. *Nature* **429**, 671–675 (2004).
43. Kholod, N. & Mustelin, T. Novel vectors for co-expression of two proteins in *E. coli*. *Biotechniques* **31**, 322–323 326–328 (2001).
44. Kapust, R.B. *et al.* Tobacco etch virus protease: mechanism of autolysis and rational design of stable mutants with wild-type catalytic proficiency. *Protein Eng.* **14**, 993–1000 (2001).
45. Van Duyn, G.D., Standaert, R.F., Karplus, P.A., Schreiber, S.L. & Clardy, J. Atomic structures of the human immunophilin FKBP-12 complexes with FK506 and rapamycin. *J. Mol. Biol.* **229**, 105–124 (1993).
46. McPherson, A. *Crystallization of Biological Macromolecules* (Cold Spring Harbor Press, Cold Spring Harbor, New York, USA, 1999).
47. Otwinowski, Z. & Minor, W. Processing of X-ray diffraction data collected in oscillation mode. *Methods Enzymol.* **276**, 307–326 (1997).
48. Schneider, T.R. & Sheldrick, G.M. Substructure solution with SHELXD. *Acta Crystallogr. D Biol. Crystallogr.* **58**, 1772–1779 (2002).
49. Fortelle, E.I. & Bricogne, G. Maximum-likelihood heavy atom parameter refinement for multiple isomorphous replacement and multiwavelength anomalous diffraction methods. *Methods Enzymol.* **276**, 472–494 (1997).
50. Terwilliger, T.C. Maximum-likelihood density modification. *Acta Crystallogr. D Biol. Crystallogr.* **56**, 965–972 (2000).
51. Perrakis, A., Morris, R. & Lamzin, V.S. Automated protein model building combined with iterative structure refinement. *Nat. Struct. Biol.* **6**, 458–463 (1999).
52. McRee, D.E. XtalView/Xfit—A versatile program for manipulating atomic coordinates and electron density. *J. Struct. Biol.* **125**, 156–165 (1999).
53. Collaborative Computational Project, Number 4. The CCP4 suite: Programs for protein crystallography. *Acta Crystallogr. D Biol. Crystallogr.* **50**, 760–763 (1994).
54. Edelhoch, H. Spectroscopic determination of tryptophan and tyrosine in proteins. *Biochemistry* **6**, 1948–1954 (1967).